Photoreduction of Carbon Dioxide to Methanol over Copper Based Zeolitic Imidazolate Framework-8: A New Generation Photocatalyst

Sonam Goyal [1,*], **Maizatul Shima Shaharun** [1,*], **Chong Fai Kait** [1], **Bawadi Abdullah** [2] and **Mariam Ameen** [3]

[1] Department of Fundamental and Applied Sciences, Universiti Teknologi PETRONAS, Seri Iskandar, Perak 32610, Malaysia; chongfaikait@utp.edu.my
[2] Chemical Engineering Department, Universiti Teknologi PETRONAS, Seri Iskandar, Perak 32610, Malaysia; bawadi_abdullah@utp.edu.my
[3] Biomass Processing Lab., Centre for Biochemical and Biofuel Research, Chemical Engineering Department, Universiti Teknologi PETRONAS, Seri Iskandar, Perak 32610, Malaysia; mariam_g02883@utp.edu.my
* Correspondence: sonam_g03236@utp.edu.my (S.G.); maizats@utp.edu.my (M.S.S.);
  Tel.: +60-16-434-2129 (S.G.); +60-12-521-0200 (M.S.S.)

Abstract: The efficient reduction of CO_2 into valuable products such as methanol, over metal-organic frameworks (MOFs) based catalyst, has received much attention. The photocatalytic reduction is considered the most economical method due to the utilization of solar energy. In this study, Copper (II)/Zeolitic Imidazolate Framework-8 (Cu/ZIF-8) catalysts were synthesized via a hydrothermal method for photocatalytic reduction of CO_2 to methanol. The synthesized catalysts were characterized by X-ray Photoelectron Spectroscopy (XPS), Field Emission Scanning Electron Microscopy (FESEM) coupled with Energy Dispersive X-ray (EDX), Ultraviolet-visible (UV-vis) spectroscopy, and X-Ray Diffraction (XRD). The host ZIF-8, treated with 2 mmol copper prepared in 2M ammonium hydroxide solution showed the highest photocatalytic activity. The crystal structures of ZIF-8 and 2Cu/ZIF-8N2 catalysts were observed as cubic and orthorhombic, respectively and the XPS analysis confirmed the deposition of Cu (II) ions over ZIF-8 surface among all the prepared catalysts. The orthorhombic structure, nano-sized crystals, morphology and Cu loading of the 2Cu/ZIF-8N2 catalyst were the core factors to influence the photocatalytic activity. The yield of Methanol was found to be 35.82 μmol/L·g after 6 h of irradiations on 2Cu/ZIF-8N2 catalyst in the wavelength range between 530–580 nm. The copper-based ZIF-8 catalyst has proven as an alternative approach for the economical photocatalytic reduction of CO_2 to CH_3OH.

Keywords: metal-organic frameworks (MOFs); photocatalytic CO_2 reduction; Cu/ZIF-8; methanol production

1. Introduction

The major environmental concern in the 21st century is global warming and carbon dioxide (CO_2) is its main contributor [1]. The efficient and economical reduction of CO_2 has received great attention in the recent past. To reduce the CO_2 concentration, several approaches have been proposed [2]. One of the most favorable and advantageous methods is the photoconversion of CO_2 into valuable fuel with the assistance of sustainable energy source such as sunlight [3]. The conversion of CO_2 into valuable fuels is one of the ways to address the global warming problem efficiently. For this purpose, researchers have emphasized on the utilization of CO_2 as an alternative feedstock to photocatalytically reduce CO_2 to methanol. The discovery of photocatalytic reduction of CO_2 over various semiconductors, for example, TiO_2 [4], nanoparticles or nanotubes [5], Pt-promoted

polyaniline-TiO_2 nanocomposites [6], graphene oxide-CuO nanocomposites [7] have been used under UV-vis illumination, however, they exhibited low photocatalytic activity and absorbed only ultraviolet range of light [8]. TiO_2 is proved to be most suitable photocatalyst of a semiconductor due to its chemical and physical stability, low-cost, non-toxicity and convenience for use. The only drawback of it is that it can only be excited by ultraviolet light and only 4% of sunlight is ultraviolet light [9,10]. Therefore, the development of photocatalyst, particularly visible light response catalyst for the efficient utilization of solar energy is hence of great significance.

The new generation catalyst which has been widely investigated since 1990 known as porous metal-organic frameworks (MOFs) [11]. MOFs are self-assembled by the coordination of metal cations/clusters with organics linkers. The MOFs can be used in several research areas such as nonlinear optics, molecular recognition, sensors, catalysis, gas storage and separation process [12]. Furthermore, application of MOFs extends to dye's degradation [13], water splitting [14], and photocatalytic CO_2 reduction or H_2 production [15]. The broad application of MOFs is mainly due to the limited micropore dispersion, high dispersion of metals, prompt mono-dispersion of nanoparticles, and high surface area. All these properties contribute to increase the catalytic activity and selectivity [16]. MOFs demonstrated ultraviolet light photoresponse with absorption peaks around 250 nm. Depending on the type of material used, the absorption bands can expend from 250 nm to 300 nm or even in (>400 nm) visible region without further stretch [17]. Zeolitic imidazolate framework-8 (ZIF-8) is a sub-class of MOF and it exhibits excellent thermochemical and structural stability towards a CO_2 reduction in water [18]. ZIF-8 also shows CO_2 adsorption capability in liquid medium towards methanol production [19]. Because of uniform pores, channels on the surface and high surface area, ZIF-8 have been used as a catalyst in photocatalytic reaction [20], Knoevenagel reaction [21], cycloadditions and condensation reactions [22]. The bandgap energy of ZIF-8 is very high (Eg = 4.9 eV) which exhibits adsorption only in the UV region [23]. Hence, there is a need to modify pure ZIF-8 to increase the reduction of CO_2, such as Zn_2GeO_4/ZIF-8 nanorods [19]. However, to the best of our knowledge, very limited work reported on new catalyst formulations for methanol production from CO_2 under visible light irradiation.

Copper metal is a good applicant for coupling with ZIF-8 due to its amphoteric nature, inexpensive and easy synthesis. Hence the compounds of Cu/ZIF-8 are expected to show better photocatalytic reaction towards methanol production. Incorporation of copper metal over ZIF-8 reduces the effective bandgap energy and shows its incidence in the visible region. It is reported that new nanomaterials can be developed to improve the catalytic properties of Cu^{2+} and chemical stability of ZIF-8 crystals [22,24]. The Cu (II) ion plays the role of a co-catalyst in the reduction of CO_2 by facilitating the transfer of charge and restricts the recombination of electrons and holes [25,26]. It has been reported that to reduce CO_2, Cu cations and Cu oxides play an active role as co-catalyst and provide as reductive locations to increase the selectively of CH_3OH [27–29]. The comparison with the Zn_2GeO_4 nanorods and Zn_2GeO_4/ZIF-8 hybrid nanorods consisting of 25 wt.% ZIF-8, Zn_2GeO_4/ZIF-8 was found to be 3.8 times higher in terms of adsorption capacity for dissolved CO_2 compared to Zn_2GeO_4 nanorods. Consequently, the photoreduction rate of CO_2 into CH_3OH was found to increase by 62% [19]. According to Zhang et al., the morphology and size of the ZIF-8 crystal can be modified and the CO_2 adsorption capacity can be increased if the concentration of ammonia is varied [30]. The ZIF-8 crystals are generally synthesized via *N,N*-dimethylformamide (DMF)) [31] and methanol [32] organic solvents. These solvents are toxic to the environment and expensive. Therefore, in this study, a nontoxic, environmentally benign and inexpensive solvent such as water is utilized as an alternative solvent to synthesize ZIF-8 material.

To explore the potential of new catalyst formulations for methanol production, Cu/ZIF-8 catalysts were synthesized by hydrothermal method. Present work reports the application of Cu/ZIF-8 catalysts in the photocatalytic reactor for the reduction of CO_2 (in continuous flow system) to methanol in the presence of water (in batch mode) under 280 W/m^2 irradiations of visible light.

2. Results and Discussion

2.1. Effect of Solvent Concentration on Cu/ZIF-8

The phase crystal structures of ZIF-8 and 2Cu/ZIF-8 with different ammonium hydroxide concentrations (2M, 3M and 4M) were determined by using powder XRD are presented in Figure 1. The XRD patterns revealed that the loading of copper imposed no significant effect on the ZIF-8 structure. As there was no significant peak of copper appeared in XRD spectra, it might be due to the relatively lower amount of Cu. It may be concluded that ammonia concentration can affect the structure, size and morphology of the catalyst, these results are also in line with FESEM images discussed in the next section. The refraction peaks of synthesized ZIF-8 are comparable with the reported literature [33].

ZIF-8 shows cubic structure in the all synthesized composites at Zn-N bond angle with crystal size 32 nm. However, 2Cu/ZIF-8N3 exhibits tetragonal structure with the crystal size of 114 nm and other two catalyst shows an orthorhombic structure where crystal size of 2Cu/ZIF-8N4 and 2Cu/ZIF-8N2 was 200 nm and 50nm, respectively, at the highest intensity peak of Cu-N bond angle in each sample. In 2Cu/ZIF-8N3, the appearance of ZIF-8 is very low due to the presence of some extra peaks of impurity of copper dinitrate(V) sesquihydrate, because it exhibits no valid relationship with crystal structure. Additionally, with the change in ammonia concentration (4M to 2M) the reduction of crystal size (as tabulated in Table A1) was observed due to further deprotonating of the unreacted imidazole ligands in the pores that accelerates the crystallization process as illustrated in Figure 2(Ad). However at excess of ammonia concentration in composite additional ammonium group would reside within the pores lead to increase of particle size [34]. It confirms that the solvent concentration can affect the crystal size of the catalysts without harmless the host material in the composite.
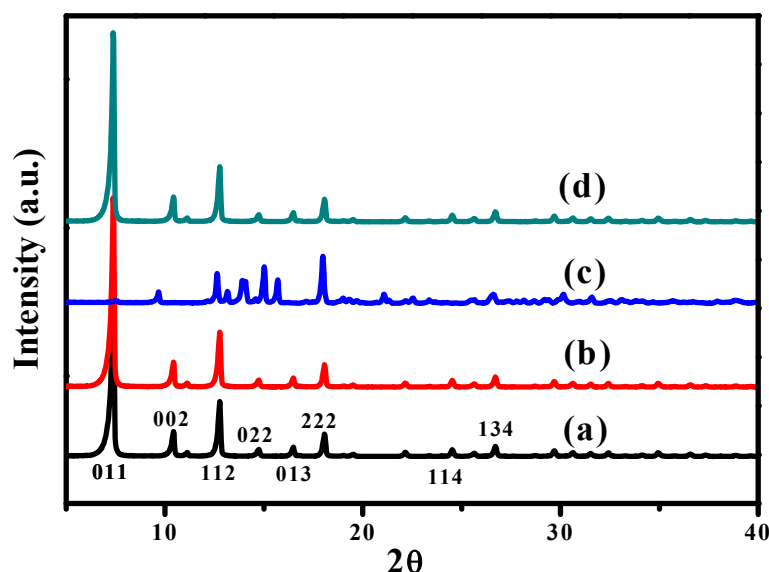
Figure 1. XRD images of (a) ZIF-8 (b) 2Cu/ZIF-8N4 (c) 2Cu/ZIF-8N3 (d) 2Cu/ZIF-8N2.

The morphological effects of ZIF-8 and 2Cu/ZIF-8 materials synthesized with different NH_4OH concentrations were determined by FESEM as shown in Figure 2(Aa–Ad). The morphology of ZIF-8 is a hexagonal cage. In addition, Figure 2(Ab–Ad) illustrates that the addition of copper over ZIF-8 shaped the rhombic dodecahedron structure, which is a typical ZIF-8 structure as reported [35]. However, the addition of Cu metal did not considerably change the structure of ZIF-8, it could be due to the low Cu loading. However, the aggregate size was significantly reduced as it is highly affected by the solvent concentration. When NH_4OH concentrations were decreased from 4M to 2M, the aggregate particle size of the catalysts was significantly decreased from 200 to 50 nm, respectively. The FESEM

image of 2Cu/ZIF-8N2 illustrates the finest morphology of the desired crystals for the photocatalytic activity. The reduction of particle size is also in line with XRD pattern as discussed earlier. In Figure 2B, FESEM dot mapping of 2Cu/ZIF-8N2 indicates the dispersion of Cu ions into the composite. Every component present in the sample structure is finely distributed by dots with a specific color. It can be seen from the Figure 2B, that Cu species are homogeneously distributed.

(a)

(b)

(c)

(d)

(A)

Electron Image 1

C Ka1_2

Cu Ka1

N Ka1_2

Zn Ka1

(B)
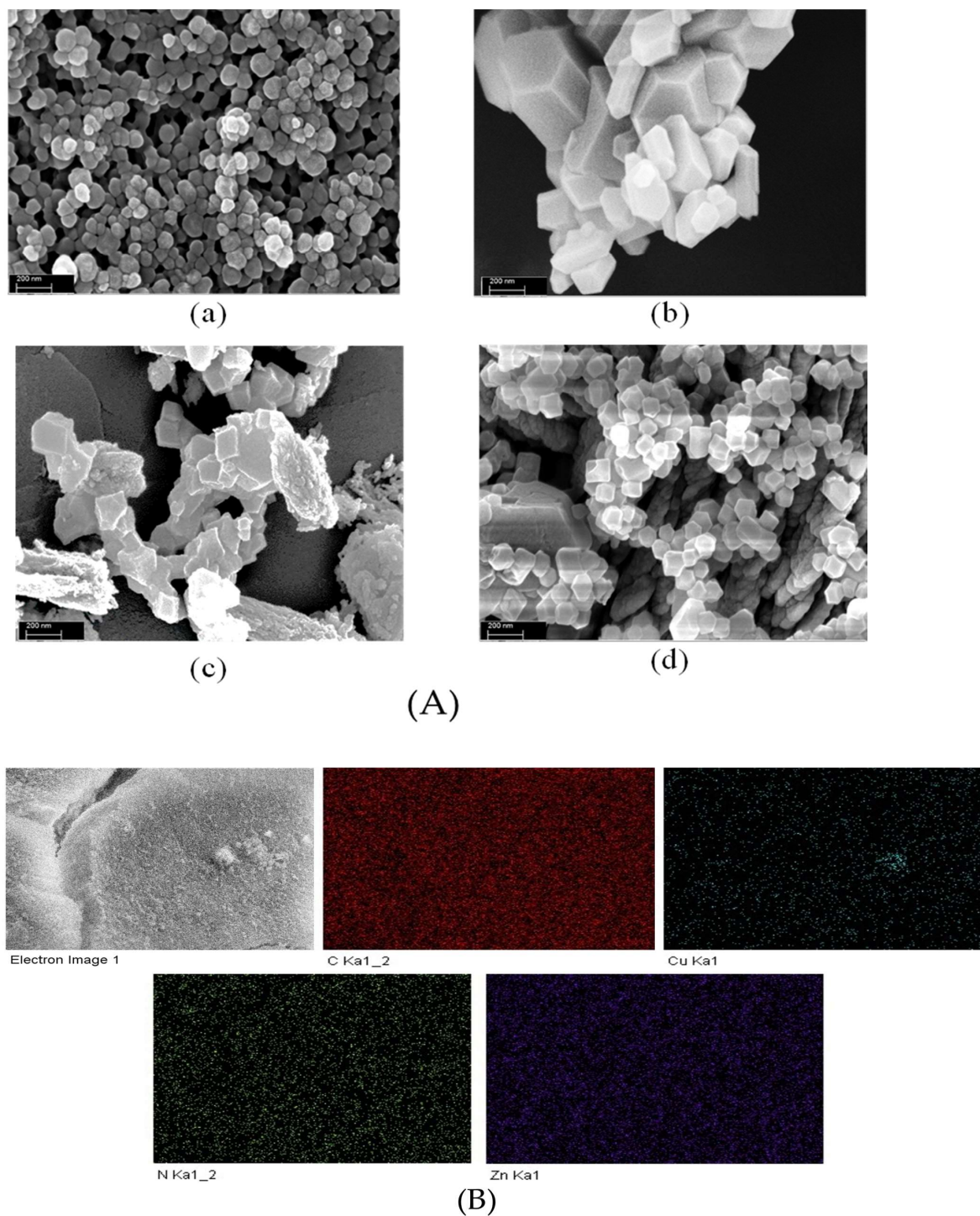
Figure 2. FESEM images of (**A**) (**a**) ZIF-8 (b) 2Cu/ZIF-8N4 (**c**) 2Cu/ZIF-8N3 (**d**) 2Cu/ZIF-8N2 and (**B**) dot mapping images of 2Cu/ZIF-8N2.

UV-vis optical absorption spectra of the materials recorded within the region from 200 to 800 nm are shown in Figure 3A. 2Cu/ZIF-8 based materials exhibit a systematic increment in the absorption intensity with a relative decrement in ammonium hydroxide concentration. The 2Cu/ZIF-8N2 shows extensive absorption peak in the visible region as compared to the other materials. In Figure 3(Ad), 2Cu/ZIF-8N2 appeared in the ultraviolet range with a sharp peak at 330 nm. The 2Cu/ZIF-8N2 shows extensive absorption peak in the visible region as compared to the other materials and the same observation were characterized by Chary et al. [36]. The origin of the broad absorption peak in the visible region is might be due to the interaction of 2M concentration of ammonium hydroxide solvent with Cu/ZIF-8. The absorption peak in 2Cu/ZIF-8N2 sample at 330 nm shows a strong interaction of N-Cu-N cluster formation, signifying the highly dispersed form of copper. Apart from that, two more absorption shoulders were observed in the current study. An absorption peak centered at 520 nm with energy band gap of 2.38 eV suggested the presence of Zn^{2+}. Similarly, the absorption band around 710 nm with energy band gap of 1.75 eV was assigned to $^2Eg \rightarrow {}^2T_2g$ transitions of Cu^{2+}, indicating octahedral symmetry of Copper. Moreover, this absorption band was also attributed to the crystalline phase of copper and d-d transitions of copper (II) ion. The bandgap of the developed catalysts is used to explore the effect of ammonium hydroxide concentration using Tauc's plots as depicted in Figure 3B. In Tauc's plot, h is Planck's constant, υ is frequency and α is absorption coefficient [37]. The decrease in NH_4OH concentration from 4M to 2M resulted in the decrease of bandgap energy from 4.58 eV for 2Cu/ZIF-8N4, 3.50 eV for 2Cu/ZIF-8N3, 1.75 eV for 2Cu/ZIF-8N2. As shown in Figure 3B, the bandgap value decreased from 4.89 eV to 1.75 eV with the addition of copper into ZIF-8 that shows smaller bandgap rather than stated by Schejn et al. [22]. Hence, it proved that the UV region of host ZIF-8 (4.89 eV) can be affected with the addition of copper and different ratio of NH_4OH solvent. It is concluded that 2Cu/ZIF-8N2 exhibits a sharp edge at 1.75 eV activating the visible region of the photocatalyst. The shift in a peak in Figure 3A depicts a strong interaction between the copper metal and ZIF-8 framework. ZIF-8 and 2Cu/ZIF-8N4 present a narrow absorption profile in the visible region compared to other two 2Cu/ZIF-8 materials. The bandgap of ZIF-8 reduced after inclusion of copper on it and shifted to lower bandgap energies with more absorbance and become active in the visible region. The results suggested that 2Cu/ZIF-8N2 can be photoexcited to create more electron−hole pairs under visible light absorbance which could lead to higher photocatalytic efficiency [28,38].

Conclusively, the significant effect of solvent concentration was observed in 2Cu/ZIF-8N2. It is concluded that by increasing the molar concentration of solvent in 2Cu/ZIF-8 catalysts significantly modified the crystal structure from cubic to orthorhombic. The effect of solvent also reduced the crystal size from 200 nm to 50 nm from 4M to 2M, respectively. To investigate the effect of Cu loading, further experiments were performed on Cu/ZIF-8N2 (2M NH_4OH concentration) to study the physiochemical properties as well as the activity of the catalysts.

(**A**)

(**B**)
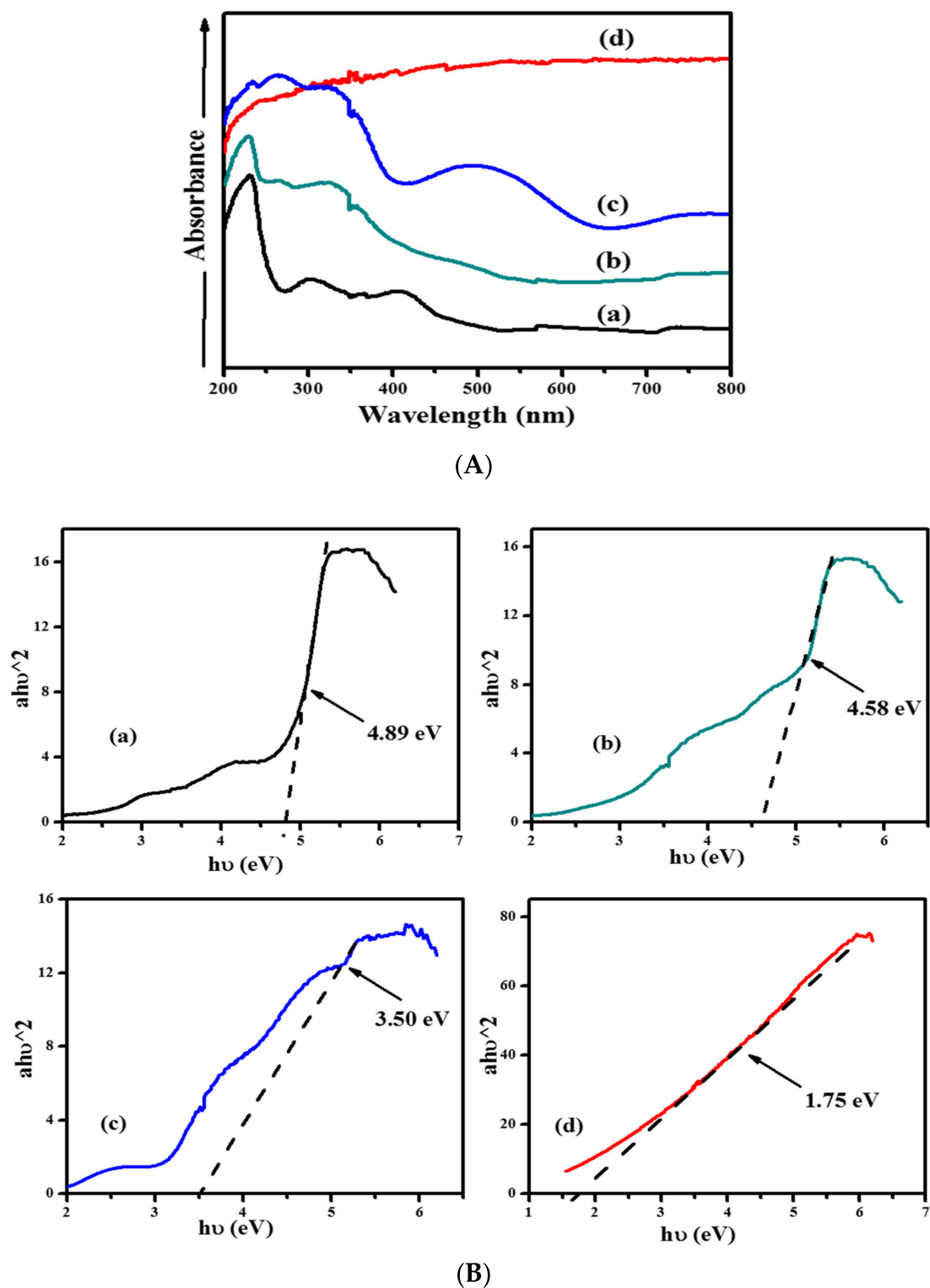
Figure 3. (**A**) UV–vis absorbance spectra of (**a**) ZIF-8 (**b**) 2Cu/ZIF-8N4 (**c**) 2Cu/ZIF-8N3 (**d**) 2Cu/ZIF-8N2 (**B**) Optical band edges of (**a**) ZIF-8 (**b**) 2Cu/ZIF-8N4 (**c**) 2Cu/ZIF-8N3 (**d**) 2Cu/ZIF-8N2.

2.2. Effect of Copper Loading on ZIF-8

The phase crystal structures of Cu/ZIF-8N2 (2M NH_4OH concentration) with different amount of copper loading (1, 2 and 3 mmol) were measured by using powder XRD as can be seen in Figure 4. The diffraction peaks of all Cu/ZIF-8N2 catalysts with different copper loadings are comparable with

the reported literature for ZIF-8 [33]. Hence, the doping of copper did not impose any significant effect on the ZIF-8 structure. However, in the 3Cu/ZIF-8N2 sample, two different peaks appeared due to the increasing copper molar ratios at 35.79° and 38.93° corresponds to Cu_2O [39] and CuO [40], respectively. While in other samples copper ion peaks were not observed due to low metal loading. ZIF-8 showed cubic structure as shown in Figures 1 and 2(Aa) whereas, other catalysts (1Cu/ZIF-8N2, 2Cu/ZIF-8N2 and 3Cu/ZIF-8N2) showed the orthorhombic structures as illustrated in Figures 4 and 5–c. A cubic lattice structure can be converted into orthorhombic lattice upon stretching [41]. Therefore, the orthorhombic structure is visible after the deposition of copper onto the ZIF-8 surface. As no other crystal structures were observed, all Cu/ZIF-8N2 catalysts with different copper loadings showed an orthorhombic structure with ICDD code: 03-065-6209. Peak broadening indicates the formation of nanosized crystals as can be clearly seen in the catalysts XRD pattern (Figure 4).

The one-sided N-Cu-N angle of a crystal lattice was observed when the framework parameters were a = 13.46 Å, b = 3.08 Å, c = 9.08 Å. All samples have a crystal size below 90 nm (Table A1) as predicted from the Scherrer Equation (Equation (11)) for the highest intensity peak of each sample.
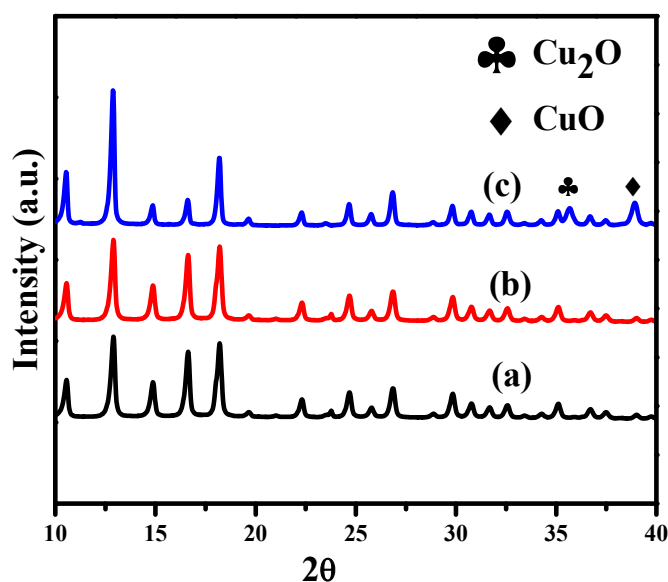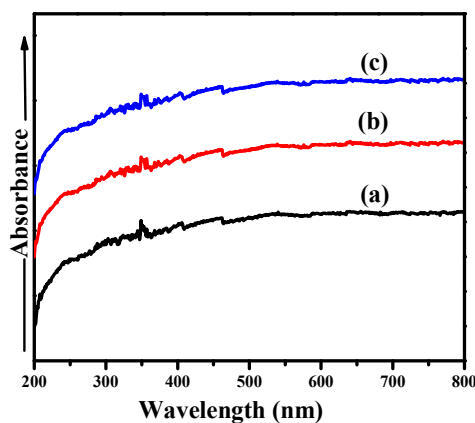

Figure 4. XRD spectra of (**a**) 1Cu/ZIF-8N2 (**b**) 2Cu/ZIF-8N2 (**c**) 3Cu/ZIF-8N2.

The topographic images of Cu/ZIF-8N2 with different amount of copper loading are presented in Figure 5a–c. FESEM images showed that, with the increase in copper loading on host materials, the surface morphology of the catalyst can be affected. However, particles are uniformly distributed and no significant effect on the particle aggregation was observed. FESEM-EDX of the 2Cu/ZIF-8N2 catalyst indicates that Cu, Zn, C and N are the four components observed on the surface of the sample as illustrated in Figure 5d. EDX and FTIR spectra of Cu/ZIF-8N2 are presented in Figures S1 and S2 respectively, which confirm the synthesis of Cu/ZIF-8 composite and presence of imidazole ring attached with metals atoms.
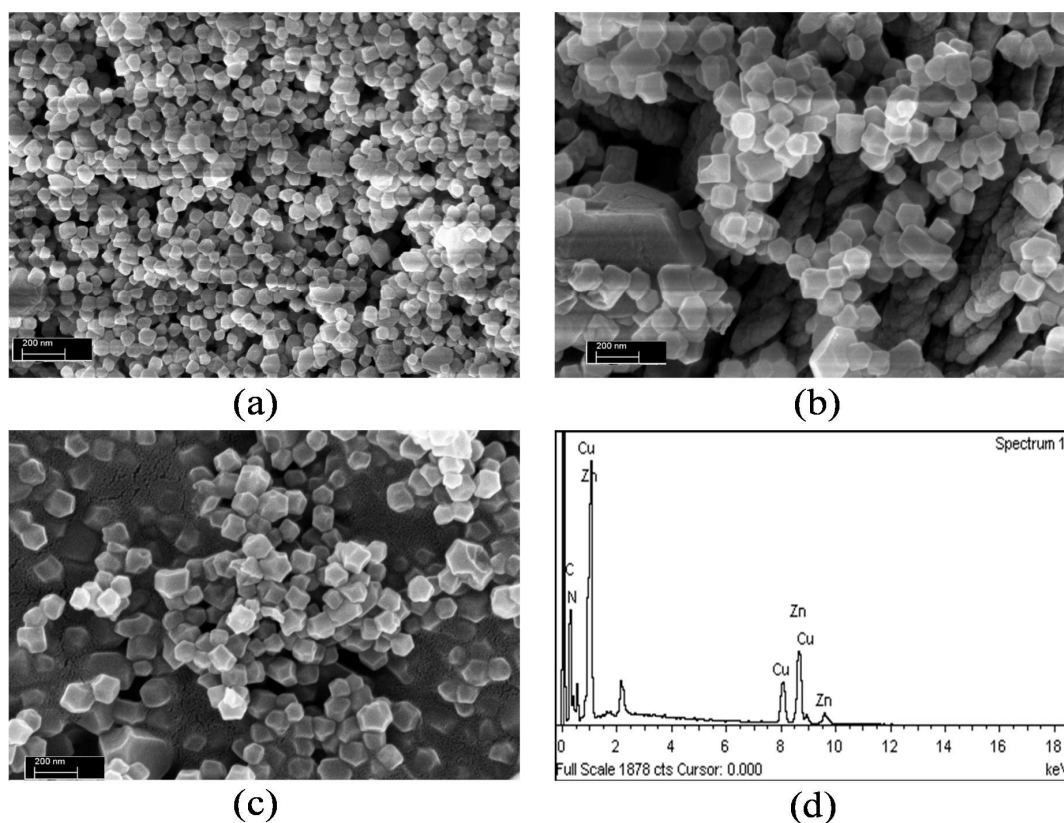
Figure 5. FESEM images of (**a**) 1Cu/ZIF-8N2 (**b**) 2Cu/ZIF-8N2 (**c**) 3Cu/ZIF-8N2 and (**d**) EDX image of 2Cu/ZIF-8N2.

The optical absorbance spectra of all Cu/ZIF-8N2 catalysts with different amount of copper loading were examined by UV-vis spectroscopy as can be seen in Figure 6. An extensive absorption spectrum can be observed for each sample. It can be found that ZIF-8 has a low absorbance in the visible region. After copper was loaded and increased consistently, the absorbance of the all Cu/ZIF-8N2 materials developed more intense in the visible region ($\lambda > 400$ nm). It is evident that there is no ending of spectrum in the visible region of all catalysts. Zhang et al. [42] studied the increment in the visible region after deposition of the metal onto the support surface. The UV-vis spectra clearly indicate that the absorption of a metal particle onto the support surface enables it to participate in the photocatalytic reaction. The formation rate and the number of electrons and holes on the surface of the photocatalyst correlate significantly with the absorbance of visible light [43]. The band gap energies of the Cu/ZIF-8N2 catalysts are mentioned in Table A1.

Figure 6. Ultra-violet visible absorbance spectra of (**a**) 1Cu/ZIF-8N2 (**b**) 2Cu/ZIF-8N2 (**c**) 3Cu/ZIF-8N2.

Furthermore, the elemental analysis was performed by XPS to confirm the loading of Cu (II) ion onto the ZIF-8 surface for each Cu/ZIF-8N2 catalyst. The spectrum in Figure 7A shows that the Cu $2p_{3/2}$ and Cu $2p_{1/2}$ peaks are located at approximately 934 eV and 954 eV, respectively, with a shake-up peak at ~943 eV for all materials. The existence of these peaks confirms the presence of Cu^{2+} in the catalyst [44]. It is well reported that Cu may exist in the form of CuO [45,46]. Whereas, in the present study, it was observed that Cu is linked with a nitrogen atom of ZIF-8 which is also confirmed with FTIR spectra (Figure S2).

The peak fitted graph is combined with the Cu2p graphs in order to show the presence of Cu^{2+} and Cu^+ ions as shown in Figure 7A. The spectra show that 2Cu/ZIF-8N2 possess the higher concentration of Cu^{2+} as compared to Cu^+. Whereas, other two catalysts exhibit comparatively higher concentration of Cu^+ which lead to lower photocatalytic activity. Another resolution spectra of Zn (II) ions is demonstrated in Figure 7B, represents two characteristics peaks at 1022.4 eV and 1045.3 eV correspond to $Zn2p_{3/2}$ and $Zn2p_{1/2}$, respectively. These binding energies confirmed the presence of Zn (II) ions attached with nitrogen in the imidazole ring [47].
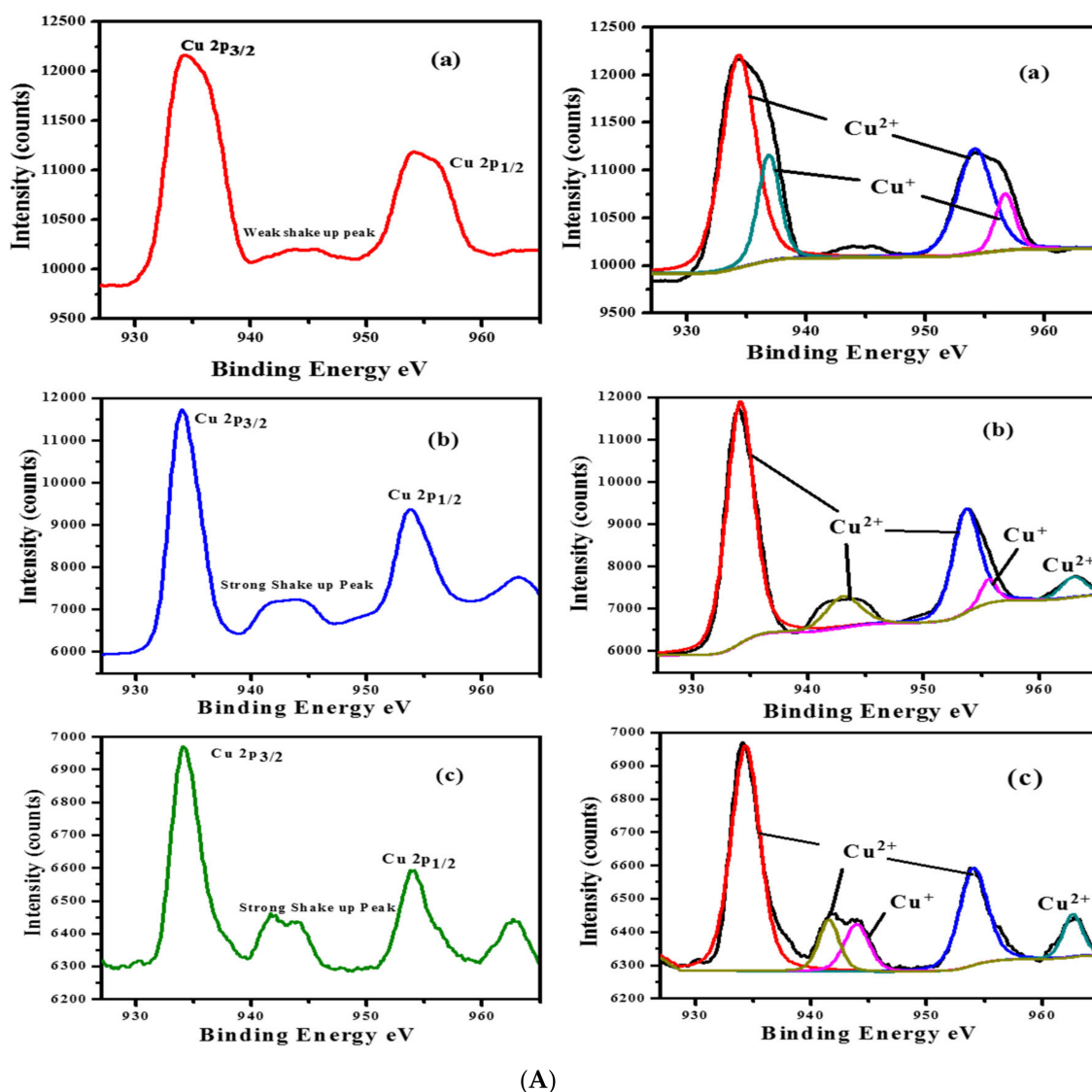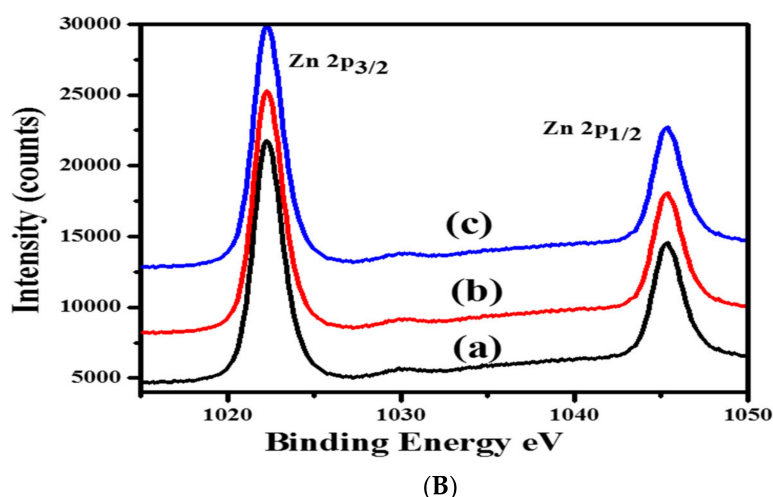

(A)

Figure 7. *Cont.*

(**B**)

Figure 7. (**A**) XPS Cu2p spectra with peak fitted graph of (**a**) 1Cu/ZIF-8N2 (**b**) 2Cu/ZIF-8N2 (**c**) 3Cu/ZIF-8N2 (**B**) Zn2p spectra of (**a**) 1Cu/ZIF-8N2 (**b**) 2Cu/ZIF-8N2 (**c**) 3Cu/ZIF-8N2.

2.3. Photocatalytic Activity

The photocatalytic reactions of all Cu/ZIF-8 catalysts were assessed by photocatalytic reduction of CO_2 in sodium hydroxide (NaOH) and sodium sulfite (Na_2SO_3) solutions in the presence of visible light for 6 h. The photocatalytic activity performed in this work is in line with the literature [48]. The use of NaOH not only enhanced the CO_2 reduction via OH radical formation but also increased the CO_2 solubility. However, Na_2SO_3 increased the proton concentration within the semiconductor particle and hole scavenging for CO_2 reduction, which increases electron's decay time. Na_2SO_3 which is working as a sacrificial agent in the supporting electrolyte, oxidized to Na_2SO_4. The experimental results revealed in Figure 8, which exhibit that the ZIF-8 was unable to generate methanol in the absence of copper whereas, other catalysts produced methanol over 6 h of irradiation time. Cu (II)/zeolitic imidazolate framework-8 offered a reductive surface to CO_2 for methanol production. 2Cu/ZIF-8N2 catalyst demonstrated the most significant activity with the yield of 35.82 μmol/L·g due to its good crystallinity, morphology and optimal chemical loadings. When the copper loading was increased to 3 mmol, the copper ions were reduced to Cu_2O as shown in Figure 4c, which degraded the separation efficiency of electron–hole pairs, consequently, declines the activity of the catalyst. XRD results confirmed that Cu/ZIF-8N2 catalysts were nanosized crystals, which are significant for photocatalytic reduction. The catalyst with high crystallinity presents fewer defects in the reaction system. Furthermore, the defected material played a vital role in the rapid recombination of photogenerated holes and electrons [49], which is responsible to reduce the photocatalytic activity. The catalytic performance of CuO and ZIF-8 was carried out at initial screening separately but no significant desire product was observed in photocatalytic reaction. In addition, we tried pure $P25-TiO_2$ in the reactor system with the same conditions and reaction solvents but there was no substantial liquid product was detected. As predictable, other hydrocarbons were formed during reaction, which were quite low to be detected.

However, in this work, methanol was the main product which is considered as value added chemicals while no other product was formed. To the best of our knowledge, this is the first experiment of methanol production in the presence of Cu/ZIF-8 catalyst.
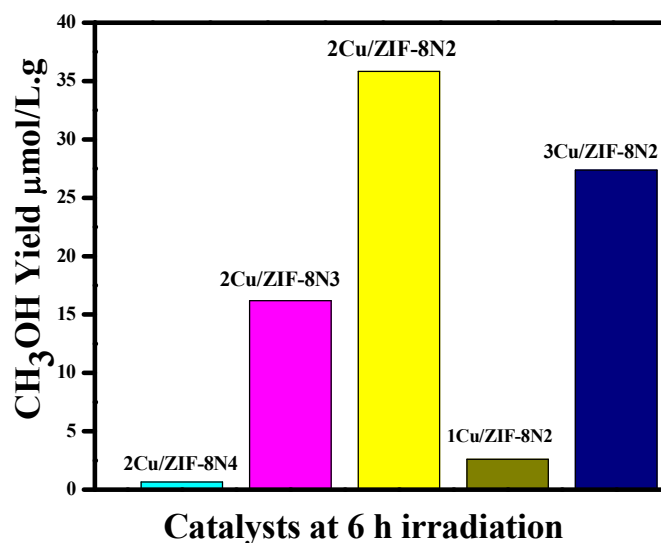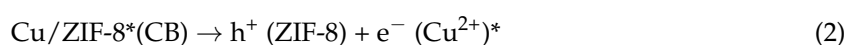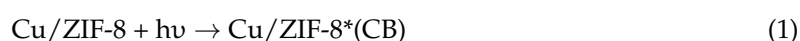
Figure 8. Photocatalytic reduction of CO_2 to CH_3OH over all Cu/ZIF-8 catalysts at 6 h irradiation.

In this study, the yield of methanol is compared with the literature data as tabulated in Table 1. Due to the different catalyst preparation method, reaction conditions and reactor setup, an exact comparison cannot be made, but a generic statement can be made that the production of methanol can be increased with the addition of metal.
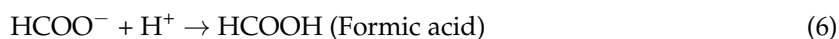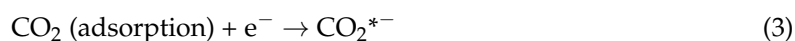
Table 1. Recent Progress in photocatalytically reduction of CO_2.

| Sr. No.	Catalyst	Reactant	Preparation Method	Reactor Condition	Product/Yield	Ref.
1	Cu porphyrin-based MOF	CO_2 and Solution of the triethylamine	Hydrothermal	300 W Xe lamp	5.97 µmol/g·h CH_3OH	[50] 2013
2	ZIF-8/Zn_2GeO_4	CO_2 and the Solution of sodium sulfite	Impregnation	500 W Xe arc lamp	2.44 µmol/g CH_3OH	[19] 2013
3	CuIm	CO_2 and solutions of sodium hydroxide and sodium sulfite	Hydrothermal	500 W, Xe lamp	1712.7 µmol/g CH_3OH	[48] 2013
4	Ti-MCM-48(25)CuTPP	CO_2 and solutions of sodium hydroxide and sodium sulfite	Impregnation	500 W Xenon Lamp	297.06 µmol/g CH_3OH	[51] 2018
5	TiO_2P25	CO_2 and solution of potassium hydrogen carbonate	Commercial	10 W UV Lamp	800 µmol/g·catal CH_3OH	[27] 2009
6	2Cu/ZIF-8N2	CO_2 and solutions of sodium hydroxide and sodium sulfite	Hydrothermal	500 W Xenon Lamp	35.82 µmol/L·g CH_3OH	This study

A photocatalytic process requires a semiconductor which absorbs the light and leads to the creation of photoexcited charge carriers. The respective photogenerated charge carriers (electron and hole) must be located at a potential negative enough for the reduction reaction and positive enough for the oxidation half-reaction. The electrons (e^-) can reduce CO_2 to CH_3OH while holes can be oxidized by water molecules into the proton. Figure 9 presents the schematic diagram of the photocatalytic reduction of CO_2 to CH_3OH over the photocatalyst. In our investigation, when the Cu/ZIF-8 catalysts were exposed to visible light, the photogenerated electron–hole pairs were created.

$$Cu/ZIF\text{-}8 + h\upsilon \rightarrow Cu/ZIF\text{-}8^*(CB) \tag{1}$$

$$Cu/ZIF\text{-}8^*(CB) \rightarrow h^+ (ZIF\text{-}8) + e^- (Cu^{2+})^* \tag{2}$$

The formation of proton (H^+) from water were carried out by Na_2SO_3, and at that point it reduces to H*, and this H^* may further reduce the CO_2.

$$CO_2 \text{ (adsorption)} + e^- \rightarrow CO_2^{*-} \tag{3}$$

$$H_2O + Na_2SO_3 \text{ (4h}^+) \rightarrow 2H^+ + Na_2SO_4 \tag{4}$$

$$CO_2^{*-} + H^+ + e^- \rightarrow HCOO^- \tag{5}$$

$$HCOO^- + H^+ \rightarrow HCOOH \text{ (Formic acid)} \tag{6}$$

$$2H_2O \text{ (4h}^+) \rightarrow O_2 + 4H^+ \tag{7}$$

Production of formic acid during this reaction is not a single step process and it further reduce to formaldehyde (HCHO) and water (H_2O) molecule with the help of electrons and protons. This reaction might be happened in the conduction band of Cu/ZIF-8 over metal atom.

$$HCOOH + 2H^+ + 2e^- \rightarrow HCHO + H_2O \tag{8}$$
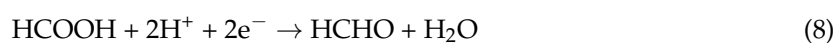
In the final step of the photocatalytic reduction of CO_2, formaldehyde reduces to the most stable liquid product, which is methanol in this study. Later on, methanol desorbs from the catalyst surface and convert to the bulk phase of liquid product.

$$HCHO + 2H^+ + 2e^- \rightarrow CH_3OH \tag{9}$$
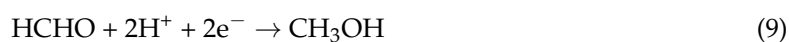
Therefore, the overall reaction in the CB of Cu/ZIF-8 is

$$CO_2 + 6H^+ + 6e^- \rightarrow CH_3OH + H_2O \tag{10}$$
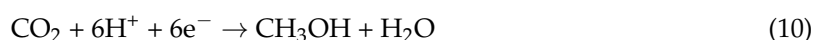
The electrons in the conduction band (CB) of 2Cu/ZIF-8N2 (E_{CB} = −1.02 V vs. NHE at pH 7) improved the separation of electron–hole pairs and prevents from recombination. The valence band (VB) potential of ZIF-8 is 2.41 V, which is more positive than the VB potential of 2Cu/ZIF-8N2 (0.72 V) thus the oxidation reaction could happen in the VB of ZIF-8. VB and CB values of all synthesized samples during this study tabulated in Table A1 which were calculated with the equation reported by Wang et al. [52].

On the basis of our findings, it could be postulated that the addition of metal to a material can alter the surface properties and overall efficiency of a material. The incorporation of metals as a charge-carrier trap enhance the reaction rate and also increase the lifespan of separated electron-hole pairs [53,54]. During the photocatalytic reaction, the electrons move from lower to higher energy level to make balance and create a Schottky barrier [55]. The Schottky barrier serves as an electron trap which stops the migration of electrons from crossing back to the valence band (VB) and therefore inhibits recombination. It was predicted that the electrons generated in the conduction bands (CB) of the Cu/ZIF-8 catalysts took place after the irradiation of visible light. This could separate the photogenerated electron–hole pairs. When pure ZIF-8 was used, no methanol was produced, the generation of methanol could be due to the reaction of CO_2 with protons and electrons ($E_{CO2/CH3OH}$ = −0.38 V) as reported [56]. A semiconductor has two main distinctive characteristics: firstly, a charge-separated state is generated when energy photons are greater than the bandgap of the material, used for the irradiation process and secondly, the mobility of the charge carriers. The charge carriers move away from the location where the separation of the charge occurs [55].
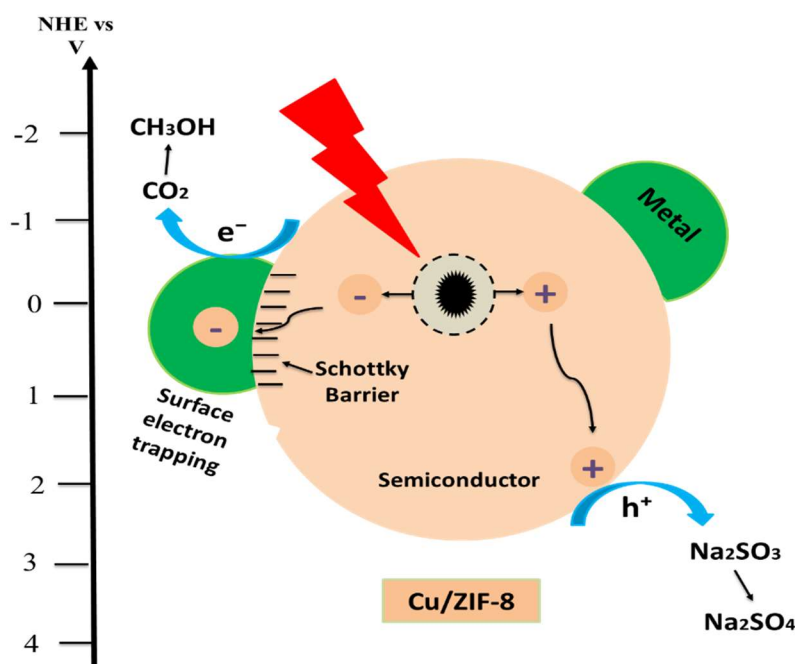
Figure 9. Schematic reduction activity of CO_2 to methanol over Cu/ZIF-8 photocatalyst under visible light irradiation.

3. Materials and Methods

Materials such as Zinc nitrate hexahydrate ($Zn(NO_3)_2 \cdot 6H_2O$), ammonia (25%), copper sulphate pentahydrate ($CuSO_4 \cdot 5H_2O$), sodium sulfite (Na_2SO_3) and sodium hydroxide (NaOH) were purchased from R&M chemicals (Essex, UK) while 2-methylimidazole (Hmim) was obtained from Sigma Aldrich (St. Louis, MO, USA). Deionized (DI) water was used in the synthesis of ZIF-8 as a solvent. No further purification of all reagents was performed and used directly.

3.1. Preparation of ZIF-8

ZIF-8 crystals were synthesized by the reported method [33] with few modifications. In 10 mL of DI water, 1.17 g of $Zn(NO_3)_2 \cdot 6H_2O$ was dissolved and 22.70 g of Hmim was added in 80 mL of DI water. The solution of zinc nitrate was added dropwise into Hmim solution with vigorous stirring for 15 min then the solution was kept aside for seven days at room temperature. The solution was separated by removing the upper liquid solution using a syringe and the remaining product was filtered. The obtained product was dried at 70 °C in an oven overnight after washing it for 4–5 times with DI water.

3.2. Synthesis of Catalysts

To synthesize Cu/ZIF-8 catalysts, the molar ratios of ZIF-8 and copper sulphate presented in Table 2 were used. The chemicals were mixed in DI water and then the solution was stirred continuously. Copper sulphate solution was mixed with the ammonium hydroxide (sacrificial agent) solutions before mixing with ZIF-8. The mixture was poured into Teflon-lined stainless-steel autoclave and then hydrothermally treated at 110 °C for two days. The solid product was obtained by filtration and washed with DI water for 3–4 times. The prepared catalyst was finally dried at 85 °C overnight. The method adopted for the synthesis of catalysts was taken from Li et al. [48].

Table 2. Catalysts composition with Cu loading and ammonium hydroxides concentrations.

S. No.	Copper Metal Loading (mmol)	ZIF-8 Loading (mmol)	Ammonium Hydroxide Concentration (M)	Catalyst Notation
1.	2	4	4	2Cu/ZIF-8N4
2.	2	4	3	2Cu/ZIF-8N3
3.	2	4	2	2Cu/ZIF-8N2
4.	1	4	2	1Cu/ZIF-8N2
5.	3	4	2	3Cu/ZIF-8N2

3.3. Characterization

The Ultraviolet-visible (UV-vis) Spectroscopy and Diffuse Reflectance Spectra (DRS) (Agilent Cary 100 UV-Vis Spectrophotometer, Santa Clara, CA, USA) were used to determine the optical absorption and bandgap energy of catalysts, respectively. The UV-vis spectra of the sample were found to be in the range of 200–800 nm. Field Emission Scanning Electron Microscopy (FESEM) and Energy Dispersive X-ray (EDX) (JEOL6340, Akishima, Tokyo, Japan) were used to investigate the morphology and element composition, respectively. The surface compositional charges were studied by X-ray Photoelectron Spectroscopy (XPS, Kratos, Manchester, UK). The analysis was carried out on a K-Alpha instrument applying a monochromatic Al Kα source (hν = 1486.6 eV, 150 W). XRD was used to identify the crystal structures of the catalysts and lattice parameters, (Bruke/D8-Advance, Karlsruhe, German; Cu Kα radiation, λ = 0.154056 nm) at room temperature at a scanning rate of 2°/min ranging from 10° to 80°. The size of crystal was calculated using the Scherrer equation (Equation (11)).

$$D = K\lambda / \beta \, Cos\theta \tag{11}$$

where, D = Crystallite size, K is crystallite shape factor (0.9), λ = 1.54 nm, β is the full width at half maximum intensity of the peak (in radian), and Cosθ is the angle (position) of the peak at 2θ.

3.4. Photocatalytic Activity

The 500-Watt optical photoreactor (Shanghai sunny scientific collaboration, Shanghai, China) configuration consists of a three-neck flask with an inner vessel for inlet and outlet water valves shown in Figure 10. The vessel volume was 500 mL. One side of the glass vessel was used for gas bubbling, another side was used for gas evacuation, while the remaining side was employed as sample collecting dock. The reactor vessel was irradiated by a 500 W Xenon lamp placed at the top of the reactor and the wavelength range was observed by intensity meter (Figure A1). An aluminum halt reflector was used to cover the vessel to enhance the visible light illumination and to prevent the intervention of ambient light. The reactor vessel was placed on the magnetic stirrer and the reaction temperature was controlled by the chiller. To confirm the photoreduction of CO_2 to methanol formation, blank tests were conducted. The blank tests involved the reactions with the catalyst in the dark and without the catalyst in the visible light.

Initially, 500 mL of NaOH and Na_2SO_3 solution was poured into the glass vessel and its pH value was measured. Pure CO_2 was bubbled into the reactor chamber for 1 h to saturate the solution. 0.5 g of catalyst was added into the reactor vessel and the resultant solution was stirred at a specific speed. The blank sample was collected without irradiation. Later, the light was turned on and eight liquid samples (5 mL each) were collected from the reactor with an interval of 1 h using a syringe. To isolate the catalyst (in particle form) from liquid samples, the catalyst-suspended samples were centrifuged. The collected samples were analyzed using GC-FID (gas chromatography-flame ionization detector, Mundelein, IL, USA) of Agilent 7890 equipped with a blood alcohol column (Agilent J&W DB-ALC column, Santa Clara, CA, USA).
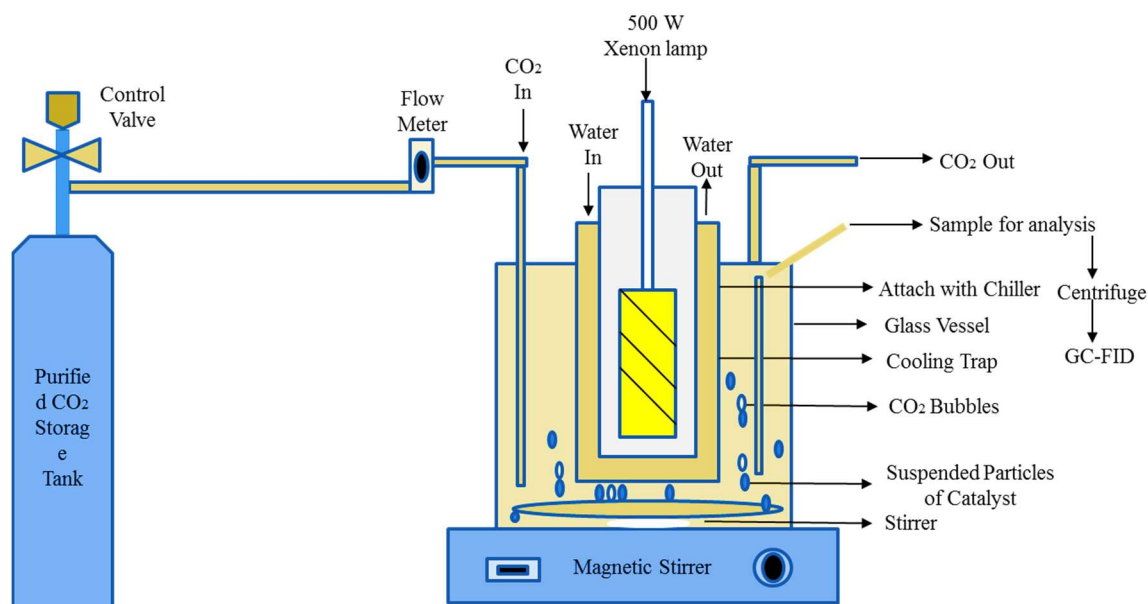
Figure 10. Schematic diagram of the reactor setup.

4. Conclusions

In this study, photocatalysts have been synthesized, characterized and tested for the reduction of CO_2 to methanol. Cu/ZIF-8 catalysts with different copper loading and ammonium hydroxide concentrations were synthesized using the hydrothermal method. The photocatalysts have been successfully tested for the reduction of CO_2 to methanol. The XRD spectra confirmed the synchronization of N-Cu-N angle with orthorhombic structure after the addition of copper metal into ZIF-8 which possessed cubic lattice structure. FESEM images also exhibited the conversion of cubic lattice to the orthorhombic structure. The UV-vis analysis indicated the increase of absorbance in the visible region after the deposition of copper and an optimized amount of solvent onto the support surface. All samples are able to produce methanol due to the presence of Cu^{2+} ions on the support surface except for ZIF-8 which is confirmed from XPS analysis. Therefore, it is confirmed that copper (II) ions play an essential role in reducing CO_2 to CH_3OH. The highest yield of methanol was found to be 35.82 μmol/L·g after 6 h of irradiation with 2 mmol Cu loading and 2M ammonium hydroxide concentration. The high yield of methanol is attributed to the synthesis method, solvent effect and Cu loading over ZIF-8. Therefore, it can be concluded that an average Cu loading, proper selection and concentration of solvent significantly affect the photocatalytic reduction of CO_2 to methanol.

Author Contributions: Writing—original draft, S.G.; Writing—review & editing, M.S.S.; Formal analysis, C.F.K.; Supervision, B.A.; Visualization, M.A.

Conflicts of Interest: The authors declare no conflict of interest.

Appendix A

Figure A1. Reactor setup attached with intensity meter.

Table A1. Summarized data of all catalyst synthesized in this study.

Sample	Crystal Size	Crystal Structure	Band Gap Energy (eV)	VB Potential (V)	CB Potential (V)	Methanol Yield (μmol/L·g)
ZIF-8	32 nm	Cubic	4.89	2.41	−2.48	No yield
2Cu/ZIF-8N4	200 nm	Orthorhombic	4.58	2.14	−2.44	0.655
2Cu/ZIF-8N3	114 nm	Tetragonal	3.50	1.6	−1.9	16.19
2Cu/ZIF-8N2	50 nm	Orthorhombic	1.75	0.72	−1.02	35.82
1Cu/ZIF-8N2	38 nm	Orthorhombic	1.80	0.75	−1.05	2.6
3Cu/ZIF-8N2	82 nm	Orthorhombic	1.65	0.67	−0.97	27.38

References

1. Ma, S.; Sadakiyo, M.; Heima, M.; Luo, R.; Haasch, R.T.; Gold, J.I.; Yamauchi, M.; Kenis, P.J. Electroreduction of carbon dioxide to hydrocarbons using bimetallic Cu-Pd catalysts with different mixing patterns. *J. Am. Chem. Soc.* **2016**, *139*, 47–50. [CrossRef] [PubMed]

2. Inoue, T.; Fujishima, A.; Konishi, S.; Honda, K. Photoelectrocatalytic reduction of carbon dioxide in aqueous suspensions of semiconductor powders. *Nature* **1979**, *277*, 637–638. [CrossRef]

3. Kimfung, L.; Martin, D.; Junwang, T. Conversion of solar energy to fuels by inorganic heterogeneous systems. *Chin. J. Catal.* **2011**, *32*, 879–890.

4. Li, K.; An, X.; Park, K.H.; Khraisheh, M.; Tang, J. A critical review of CO_2 photoconversion: Catalysts and reactors. *Catal. Today* **2014**, *224*, 3–12. [CrossRef]

5. Xie, S.; Wang, Y.; Zhang, Q.; Fan, W.; Deng, W.; Wang, Y. Photocatalytic reduction of CO_2 with H_2O: Significant enhancement of the activity of Pt–TiO_2 in CH_4 formation by addition of MgO. *Chem. Commun.* **2013**, *49*, 2451–2453. [CrossRef] [PubMed]

6. Liu, G.; Xie, S.; Zhang, Q.; Tian, Z.; Wang, Y. Carbon dioxide-enhanced photosynthesis of methane and hydrogen from carbon dioxide and water over Pt-promoted polyaniline–TiO_2 nanocomposites. *Chem. Commun.* **2015**, *51*, 13654–13657. [CrossRef] [PubMed]

7. Gusain, R.; Kumar, P.; Sharma, O.P.; Jain, S.L.; Khatri, O.P. Reduced graphene oxide–CuO nanocomposites for photocatalytic conversion of CO_2 into methanol under visible light irradiation. *Appl. Catal. B* **2016**, *181*, 352–362. [CrossRef]

8. Shi, H.; Chen, G.; Zhang, C.; Zou, Z. Polymeric g-C_3N_4 coupled with $NaNbO_3$ nanowires toward enhanced photocatalytic reduction of CO_2 into renewable fuel. *ACS Catal.* **2014**, *4*, 3637–3643. [CrossRef]

9. Li, H.; Li, C.; Han, L.; Li, C.; Zhang, S. Photocatalytic reduction of CO_2 with H_2O on CuO/TiO_2 catalysts. *Energy Sources* **2016**, *38*, 420–426. [CrossRef]

10. Sun, Q.; Lv, K.; Zhang, Z.; Li, M.; Li, B. Effect of contact interface between TiO_2 and $g\text{-}C_3N_4$ on the photoreactivity of $g\text{-}C_3N_4/TiO_2$ photocatalyst:(0 0 1) vs. (1 0 1) facets of TiO_2. *Appl. Catal. B.* **2015**, *164*, 420–427.

11. Eddaoudi, M.; Sava, D.F.; Eubank, J.F.; Adil, K.; Guillerm, V. Zeolite-like metal–organic frameworks (ZMOFs): Design, synthesis, and properties. *Chem. Soc. Rev.* **2015**, *44*, 228–249. [CrossRef] [PubMed]

12. McGuire, C.V.; Forgan, R.S. The surface chemistry of metal–organic frameworks. *Chem. Commun.* **2015**, *51*, 5199–5217. [CrossRef] [PubMed]

13. Wang, C.-C.; Li, J.-R.; Lv, X.-L.; Zhang, Y.-Q.; Guo, G. Photocatalytic organic pollutants degradation in metal–organic frameworks. *Energy Environ. Sci.* **2014**, *7*, 2831–2867. [CrossRef]

14. Meyer, K.; Ranocchiari, M.; van Bokhoven, J.A. Metal organic frameworks for photo-catalytic water splitting. *Energy Environ. Sci.* **2015**, *8*, 1923–1937. [CrossRef]

15. Wang, S.; Wang, X. Multifunctional metal–organic frameworks for photocatalysis. *Small* **2015**, *11*, 3097–3112. [CrossRef] [PubMed]

16. Zhao, Y.; Zhang, J.; Song, J.; Li, J.; Liu, J.; Wu, T.; Zhang, P.; Han, B. Ru nanoparticles immobilized on metal–organic framework nanorods by supercritical CO_2-methanol solution: Highly efficient catalyst. *Green Chem.* **2011**, *13*, 2078–2082. [CrossRef]

17. Zhang, T.; Lin, W. Metal–organic frameworks for artificial photosynthesis and photocatalysis. *Chem. Soc. Rev.* **2014**, *43*, 5982–5993. [CrossRef] [PubMed]

18. Phan, A.; Doonan, C.J.; Uribe-Romo, F.J.; Knobler, C.B.; O'keeffe, M.; Yaghi, O.M. Synthesis, structure, and carbon dioxide capture properties of zeolitic imidazolate frameworks. *Acc. Chem. Res.* **2010**, *43*, 58–67. [CrossRef] [PubMed]

19. Liu, Q.; Low, Z.-X.; Li, L.; Razmjou, A.; Wang, K.; Yao, J.; Wang, H. $ZIF\text{-}8/Zn_2GeO_4$ nanorods with an enhanced CO_2 adsorption property in an aqueous medium for photocatalytic synthesis of liquid fuel. *J. Mater. Chem. A* **2013**, *1*, 11563–11569. [CrossRef]

20. Jing, H.-P.; Wang, C.-C.; Zhang, Y.-W.; Wang, P.; Li, R. Photocatalytic degradation of methylene blue in ZIF-8. *RSC Adv.* **2014**, *4*, 54454–54462. [CrossRef]

21. Tran, U.P.; Le, K.K.; Phan, N.T. Expanding applications of metal–organic frameworks: Zeolite imidazolate framework ZIF-8 as an efficient heterogeneous catalyst for the knoevenagel reaction. *ACS Catal.* **2011**, *1*, 120–127. [CrossRef]

22. Schejn, A.; Aboulaich, A.; Balan, L.; Falk, V.; Lalevée, J.; Medjahdi, G.; Aranda, L.; Mozet, K.; Schneider, R. Cu^{2+}-doped zeolitic imidazolate frameworks (ZIF-8): Efficient and stable catalysts for cycloadditions and condensation reactions. *Catal. Sci. Technol.* **2015**, *5*, 1829–1839. [CrossRef]

23. Yang, X.; Wen, Z.; Wu, Z.; Luo, X. Synthesis of ZnO/ZIF-8 hybrid photocatalysts derived from ZIF-8 with enhanced photocatalytic activity. *Inorg. Chem. Front.* **2018**, *5*, 687–693. [CrossRef]

24. Dutta, T.; Bagchi, D.; Pal, S.K. Bimetallic zeolitic imidazolate framework as an active excipient of curcumin under physiological condition. *Biomed. Phys. Eng. Exp.* **2018**, *4*, 055004. [CrossRef]

25. Wang, S.; Yao, W.; Lin, J.; Ding, Z.; Wang, X. Cobalt Imidazolate Metal–Organic Frameworks Photosplit CO_2 under Mild Reaction Conditions. *Angew. Chem.* **2014**, *126*, 1052–1056. [CrossRef]

26. Wang, Z.; Teramura, K.; Hosokawa, S.; Tanaka, T. Photocatalytic conversion of CO_2 in water over Ag-modified $La_2Ti_2O_7$. *Appl. Catal. B* **2015**, *163*, 241–247. [CrossRef]

27. Slamet, H.W.N.; Purnama, E.; Riyani, K.; Gunlazuardi, J. Effect of copper species in a photocatalytic synthesis of methanol from carbon dioxide over copper-doped titania catalysts. *World Appl. Sci. J.* **2009**, *6*, 112–122.

28. Sun, D.; Fu, Y.; Liu, W.; Ye, L.; Wang, D.; Yang, L.; Fu, X.; Li, Z. Studies on Photocatalytic CO_2 Reduction over NH_2-Uio-66 (Zr) and Its Derivatives: Towards a Better Understanding of Photocatalysis on Metal–Organic Frameworks. *Chem. Eur. J.* **2013**, *19*, 14279–14285. [CrossRef] [PubMed]

29. Xiang, T.; Xin, F.; Chen, J.; Wang, Y.; Yin, X.; Shao, X. Selective photocatalytic reduction of CO_2 to methanol in CuO-loaded $NaTaO_3$ nanocubes in isopropanol. *Beilstein J. Nanotech.* **2016**, *7*, 776. [CrossRef] [PubMed]

30. Zhang, Z.; Xian, S.; Xi, H.; Wang, H.; Li, Z. Improvement of CO_2 adsorption on ZIF-8 crystals modified by enhancing basicity of surface. *Chem. Eng. Sci.* **2011**, *66*, 4878–4888. [CrossRef]

31. Park, K.S.; Ni, Z.; Côté, A.P.; Choi, J.Y.; Huang, R.; Uribe-Romo, F.J.; Chae, H.K.; O'Keeffe, M.; Yaghi, O.M. Exceptional chemical and thermal stability of zeolitic imidazolate frameworks. *Proc. Natl. Acad. Sci. USA* **2006**, *103*, 10186–10191. [CrossRef] [PubMed]

32. Cravillon, J.; Nayuk, R.; Springer, S.; Feldhoff, A.; Huber, K.; Wiebcke, M. Controlling zeolitic imidazolate framework nano-and microcrystal formation: Insight into crystal growth by time-resolved in situ static light scattering. *Chem. Mater.* **2011**, *23*, 2130–2141. [CrossRef]

33. Pan, Y.; Liu, Y.; Zeng, G.; Zhao, L.; Lai, Z. Rapid synthesis of zeolitic imidazolate framework-8 (ZIF-8) nanocrystals in an aqueous system. *Chem. Commun.* **2011**, *47*, 2071–2073. [CrossRef] [PubMed]

34. Khan, I.U.; Othman, M.H.D.; Jilani, A.; Ismail, A.F.; Hashim, H.; Jaafar, J.; Rahman, M.A.; Rehman, G.U. Economical, environmental friendly synthesis, characterization for the production of zeolitic imidazolate framework-8 (ZIF-8) nanoparticles with enhanced CO_2 adsorption. *Arab. J. Chem.* **2018**, *11*, 1072–1083. [CrossRef]

35. Wu, H.; Qian, X.; Zhu, H.; Ma, S.; Zhu, G.; Long, Y. Controlled synthesis of highly stable zeolitic imidazolate framework-67 dodecahedra and their use towards the templated formation of a hollow Co_3O_4 catalyst for CO oxidation. *RSC Adv.* **2016**, *6*, 6915–6920. [CrossRef]

36. Chary, K.V.R.; Sagar, G.V.; Naresh, D.; Seela, K.K.; Sridhar, B. Characterization and Reactivity of Copper Oxide Catalysts Supported on TiO_2-ZrO_2. *J. Phy. Chem. B* **2005**, *109*, 9437–9444. [CrossRef] [PubMed]

37. Goyal, S.; Shaharun, M.S.; Kait, C.F. Characterization of copper (ii)-zirconium (iv)-imidazolate framework synthesized by hydrothermal method. *IIOAB J.* **2016**, *7*, 5.

38. Jeyalakshmi, V.; Mahalakshmy, R.; Krishnamurthy, K.; Viswanathan, B. *Titania Based Catalysts for Photoreduction of Carbon Dioxide: Role of Modifiers*; NISCAIR-CSIR: New Delhi, India, 2012.

39. Li, H.; Lei, Y.; Huang, Y.; Fang, Y.; Xu, Y.; Zhu, L.; Li, X. Photocatalytic reduction of carbon dioxide to methanol by Cu_2O/SiC nanocrystallite under visible light irradiation. *J. Nat. Gas Chem.* **2011**, *20*, 145–150. [CrossRef]

40. Uddin, M.R.; Khan, M.R.; Rahman, M.W.; Yousuf, A.; Cheng, C.K. Photocatalytic reduction of CO_2 into methanol over $CuFe_2O_4/TiO_2$ under visible light irradiation. *React. Kinet. Mech. Catal.* **2015**, *116*, 589–604. [CrossRef]

41. Grosu, Y.; Renaudin, G.; Eroshenko, V.; Nedelec, J.-M.; Grolier, J.-P. Synergetic effect of temperature and pressure on energetic and structural characteristics of {ZIF-8+ water} molecular spring. *Nanoscale* **2015**, *7*, 8803–8810. [CrossRef] [PubMed]

42. Zhang, Y.; Li, Q.; Liu, C.; Shan, X.; Chen, X.; Dai, W.; Fu, X. The promoted effect of a metal-organic frameworks (ZIF-8) on Au/TiO_2 for CO oxidation at room temperature both in dark and under visible light irradiation. *Appl. Catal. B* **2018**, *224*, 283–294. [CrossRef]

43. Qin, S.; Xin, F.; Liu, Y.; Yin, X.; Ma, W. Photocatalytic reduction of CO_2 in methanol to methyl formate over $CuO–TiO_2$ composite catalysts. *J. Colloid Interface Sci.* **2011**, *356*, 257–261. [CrossRef] [PubMed]

44. Jiang, X.; Lin, Q.; Zhang, M.; He, G.; Sun, Z. Microstructure, optical properties, and catalytic performance of Cu_2O-modified ZnO nanorods prepared by electrodeposition. *Nanoscale Res. Lett.* **2015**, *10*, 30. [CrossRef] [PubMed]

45. Li, G.; Dimitrijevic, N.M.; Chen, L.; Rajh, T.; Gray, K.A. Role of surface/interfacial Cu^{2+} sites in the photocatalytic activity of coupled $CuO-TiO_2$ nanocomposites. *J. Phy. Chem. C* **2008**, *112*, 19040–19044. [CrossRef]

46. Colon, G.; Maicu, M.; Hidalgo, M.S.; Navio, J. Cu-doped TiO_2 systems with improved photocatalytic activity. *Appl. Catal. B* **2006**, *67*, 41–51. [CrossRef]

47. Yang, M.; Zhu, L.; Li, Y.; Cao, L.; Guo, Y. Asymmetric interface band alignments of Cu_2O/ZnO and ZnO/Cu_2O heterojunctions. *J. Alloy. Compd.* **2013**, *578*, 143–147. [CrossRef]

48. Li, J.; Luo, D.; Yang, C.; He, S.; Chen, S.; Lin, J.; Zhu, L.; Li, X. Copper (II) imidazolate frameworks as highly efficient photocatalysts for reduction of CO_2 into methanol under visible light irradiation. *J. Solid State Chem.* **2013**, *203*, 154–159. [CrossRef]

49. Kudo, A.; Miseki, Y. Heterogeneous photocatalyst materials for water splitting. *Chem. Soc. Rev.* **2009**, *38*, 253–278. [CrossRef] [PubMed]

50. Liu, Y.; Yang, Y.; Sun, Q.; Wang, Z.; Huang, B.; Dai, Y.; Qin, X.; Zhang, X. Chemical adsorption enhanced CO_2 capture and photoreduction over a copper porphyrin based metal organic framework. *ACS Appl. Mater. Interfaces* **2013**, *5*, 7654–7658. [CrossRef] [PubMed]

51. Nadeem, S.; Mumtaz, A.; Mumtaz, M.; Mutalib, M.A.; Shaharun, M.S.; Abdullah, B. Visible light driven CO_2 reduction to methanol by Cu-porphyrin impregnated mesoporous Ti-MCM-48. *J. Mol. Liq.* **2018**. [CrossRef]

52. Wang, J.; Chen, K.; Shen, Y.; Wang, X.; Guo, Y.; Zhou, X.; Bai, R. Enhanced photocatalytic degradation for organic pollutants by a novel m-Bi_2O_4/$Bi_2O_2CO_3$ photocatalyst under visible light. *Res. Chem. Intermediat.* **2018**, *44*, 3061–3079. [CrossRef]

53. Ren, M.; Valsaraj, K. Inverse opal titania on optical fiber for the photoreduction of CO_2 to CH_3OH. *Int. J. Chem. React. Eng.* **2009**, *7*. [CrossRef]

54. Usubharatana, P.; McMartin, D.; Veawab, A.; Tontiwachwuthikul, P. Photocatalytic process for CO_2 emission reduction from industrial flue gas streams. *Ind. Eng. Chem. Res.* **2006**, *45*, 2558–2568. [CrossRef]

55. Linsebigler, A.L.; Lu, G.; Yates, J.T., Jr. Photocatalysis on TiO_2 surfaces: Principles, mechanisms, and selected results. *Chem. Rev.* **1995**, *95*, 735–758. [CrossRef]

56. Tahir, M.; Tahir, B.; Amin, N.A.S.; Alias, H. Selective photocatalytic reduction of CO_2 by H_2O/H_2 to CH_4 and CH_3OH over Cu-promoted In_2O_3/TiO_2 nanocatalyst. *Appl. Surf. Sci.* **2016**, *389*, 46–55. [CrossRef]